

# Effect of Contact Geometry on Spin Transport in Amine-Ended Single-Molecule Magnetic Junctions

Kuan-Rong Chiang and Yu-Hui Tang\*

Cite This: *ACS Omega* 2021, 6, 19386–19391

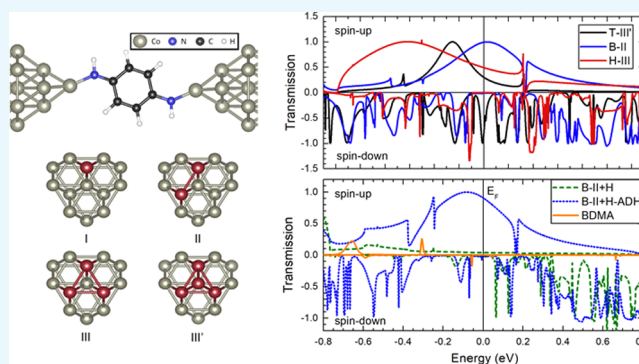
Read Online

ACCESS |

Metrics &amp; More

Article Recommendations

**ABSTRACT:** We employ the first-principles calculation with non-equilibrium Green's function method to comprehensively investigate the crucial role of interfacial geometry in spin transport properties of Co/1,4-benzenediamine (BDA)/Co single-molecule magnetic junctions (SMMJs). Two bonding mechanisms are proposed for the hard–hard Co–N coupling: (1) the covalent bonding between the H-dissociated amine linker and spin-polarized Co apex atoms and (2) the dative interaction between the H-non-dissociated (denoted by +H) amine linker and Co apex atoms. The former covalent contact dominates the  $\pi$ -resonance interfacial spin selection that can be well preserved in H-dissociated cases regardless of the choice of top, bridge, and hollow contact sites. From our detailed analyses of spin-polarized transmission spectra, local density of states, and molecular density of states, the underlying mechanism is that the strong hybridization between Co-d, N-p, and the  $\pi$ -orbital of the phenyl ring in dissociated cases renders the 2-fold HOMO (4-fold LUMO) of the central molecule closer to the Fermi energy. In contrast, the enlarged Co–N bond length of the latter dative contact in the H-non-dissociated case not only destroys the spinterface coupling but also blocks the spin injection. This theoretical work may provide vital and practical insights to illustrate the spin transport property in real amine-ended SMMJs since the contact geometries and interfacial bond mechanisms remain unclear during the breaking junction technique.



## INTRODUCTION

To reach the ultimate goal of maximizing the efficiency in electronic devices,<sup>1–8</sup> single-molecule junctions (SMJs) have attracted intensive attention due to their diversity and flexibility, and have been successfully fabricated by the scanning tunneling microscopy breaking junction process,<sup>9,10</sup> the mechanically controllable breaking junction<sup>11</sup> process, and the self-assembled monolayer fabrication.<sup>12,13</sup> SMJs consist of three distinct components: the electrode, linker, and central molecule; the linker group (also known as the anchor group or contact group) connects the central molecule to the electrodes, and the linker typically binds to the electrode, that is, the most used Au electrode, either through the dative interaction or via the covalent bonding. Based on Pearson's principle of hard and soft acids and bases,<sup>14</sup> the weaker coupling between the soft metal (Au) and hard base (N) provides the dative contact involving a lone pair donors of the H-non-dissociated amine linker selectively binding to the undercoordinated Au adatom,<sup>15–17</sup> which may limit the contact geometry and narrows the charge-transfer channels. In contrast, the thiol linker is one of the most appropriate candidates for charge transport in SMJs due to its excellent interfacial coupling and ductility. Such strong coupling between the soft metal (Au) and soft base (S) energetically produces the covalent contact

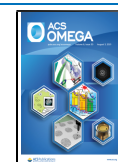
from the H-dissociated thiol linker on Au surfaces<sup>18,19</sup> and can further show broad conductance features owing to the large variability in the linker–electrode contact geometry.<sup>20,21</sup>

Besides the charge transfer, the so-called spinterface<sup>22–24</sup> effect between the ferromagnetic electrode and organic molecules provides rich physics to closely correlate interfacial chemical bonding with spin transport properties. One crucial and important issue is how to achieve highly spin-polarized currents via the spin filtering effect<sup>25–28</sup> in nanoscale organic-based spintronic devices. Recent theoretical works proposed a new type of single-molecule magnetic junctions (SMMJs) with strong hard–hard coupling between the amine linker and ferromagnetic electrode, which provide an additional degree of freedom of spin to control the electronic signal since the spin momentum of electrons can be well preserved in a diffusion length of hundreds of nanometers due to weak spin–orbit

Received: February 20, 2021

Accepted: July 13, 2021

Published: July 25, 2021



coupling. The amine linker plays an important role to provide efficient spin-selective transport properties,<sup>29,30</sup> anomalous magnetoresistance,<sup>31</sup> and the giant nonlocal field-like spin torque effect.<sup>32</sup> Unlike the dative interaction between amine and Au in nonmagnetic SMJs, the strong coupling between the hard metal (Co) and hard base (N) in SMMJs instead favors the covalent bonding between the H-dissociated amine linker and Co adatom and may even provide variability in the linker–electrode contact geometry, which are crucial but remain unclear during the fabrication of real SMMJs, especially for breaking junction techniques.

In this study, we propose prototypical Co/1,4-benzenediamine (BDA)/Co SMMJs as presented in Figure 1. The first-

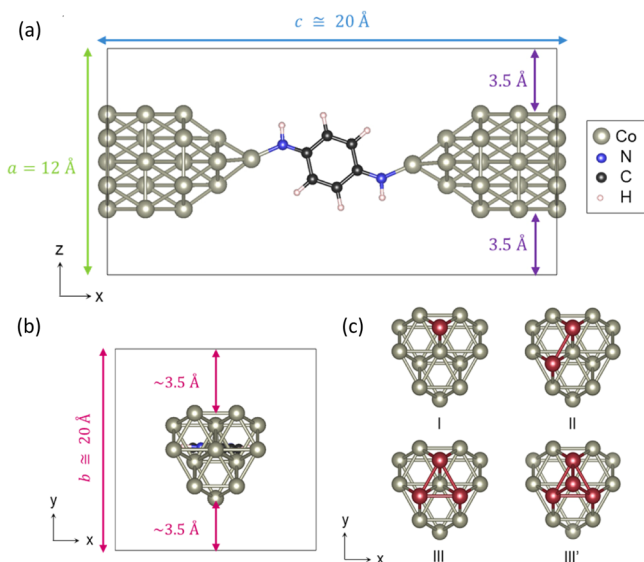


**Figure 1.** (a) Top view and (b) side view of the junction geometry for the H-dissociated T-III' case of amine-ended Co/BDA/Co SMMJ. (c) Front view of single-electrode structures, where the number of apex atoms is labeled as I, II, III, and III' for one to three plus one tip atoms. In this case, the nitrogen atom can contact on top, bridge, hollow sites of the apex atoms, labeled as T, B, and H, respectively.

principles calculation with nonequilibrium Green's function method is employed to comprehensively investigate the crucial role of interfacial geometry in spin transport of amine-ended SMMJs with various kinds of contact geometries, such as the number and symmetry of Co apex atoms (I, II, III, III') and the contact site of the N-ion (T, B, H). This gives two bonding mechanisms for the Co–N bond: (1) the covalent bonding between the H-dissociated amine linker and Co apex atoms in the T-III', B-II, and H-III cases and (2) the dative interaction between the H-non-dissociated (denoted by +H) amine linker and Co apex atoms in the T-III'+H and B-II+H cases. It is interesting to find that the former covalent contact in the H-dissociated case assists the spinterface effect and provides broad spin-polarized channels to allow the spin injection from the Co electrode via the N-linker into the central phenyl ring. However, the enlarged Co–N bond length in the latter dative contact not only dramatically destroys the spinterface coupling but also blocks the spin injection. The underlying mechanism can be understood by the fact that the strong (weak) hybridization between Co-d, N-p<sub>y</sub>, and the  $\pi$ -orbital of the central phenyl ring in H-dissociated (H-non-dissociated) amine-ended SMMJs renders the 2-fold HOMO (4-fold LUMO) of the central molecule closer to the Fermi energy.

## COMPUTATIONAL DETAILS

The Vienna ab initio simulation package<sup>33–36</sup> with density functional theory (DFT) based on generalized gradient approximation in the Perdew, Burke, and Ernzerhof<sup>37</sup> form is employed for structure relaxation in the parallel magnetic configuration. To simulate the contact condition during the breaking junction technique, we gradually change the distance between two electrodes by 0.1 Å of each step and optimize the junction with full relaxation of apex atoms and the central molecule. The vacuum layer remains at 7 Å in the *x*- and *y*-directions to prevent coupling between SMMJs. The lattice constant of the cobalt nanowire is chosen as 2.5 Å, and the Co apex atoms and central molecules are fully relaxed with a force criterion of 0.02 eV/Å. The cutoff energy of the plane wave basis set is 700 eV, the total energy difference for electronic steps is 10<sup>−5</sup> eV, and the  $\Gamma$ -point sampling is considered.

For the spin-polarized transport calculation, the two-probe model with DFT and nonequilibrium Green's function (NEGF) formalism is implemented in the Nanodcal transport package.<sup>38–40</sup> The double- $\zeta$  double-polarized basis set of local numerical orbitals is applied to all ions. The lateral separation between junctions is 15 Å to prevent the inter-junction interactions. The *k*-space sampling is 1  $\times$  1 1n100 and the  $\Gamma$ -point for the semi-infinite Co electrode and device self-consistent calculations, respectively.

## RESULTS AND DISCUSSION

We first discuss the covalent contact in the H-dissociated T-III', B-II, and H-III cases with the parallel magnetic configuration, whose spin-polarized transmission spectra are shown in the left panel of Figure 2. The pronounced  $\pi$ -resonant spin-up channel near the Fermi energy ( $E_F = 0.0$  eV) in all three top (T-III'), bridge (B-II), and hollow (H-III) contact sites as long as the H-ion is dissociated to form the covalent Co–N bond. According to the spin-polarized differential local density of states (LDOS) shown in Figure 2a, such a broad  $\pi$ -resonant spin-up channel is dominated by the N-p<sub>y</sub> ( $\pi$ ) hybridization between the  $\pi$ -orbital of the central molecule and the Co-d orbital in the T-III' case. For the dissociated B-II and H-III cases shown in Figure 2c,d, rather than pure N-p<sub>y</sub>( $\pi$ ) hybridization, both N-p<sub>x</sub> and N-p<sub>y</sub> orbitals contribute to the hybridization between the Co electrode and central molecule. As long as the N-linker can form a  $\pi$ -direction orbital, the spin-polarized electron will have an overwhelming tendency to pass through the central molecule. However, this additional N-p<sub>x</sub> orbital is not useless at all; the pronounced peak can be further extended in this way by contacting on the hollow site. In addition, the spin-down transmission is spiky in all three cases due to the great amount of spin-down electrons injected from the Co electrode near  $E_F$ , but only few of them can pass through the weak  $\pi$ -resonant spin-down channel, as displayed in Figure 2b.

On the other hand, we propose the dative contact in the H-non-dissociated B-II+H case and employ the first-principles calculation to optimize its junction structure. The enlarged N–Co bond length, that is,  $d_{N-Co}$  is 1.84 Å (B-II) and 1.99 Å (B-II+H), implies the dative contact involving a lone pair donors of the H-non-dissociated amine linker selectively binding to the undercoordinated Co apex atoms. This breaks the hybridization between spin-up Co-d, N-p<sub>y</sub>, and the  $\pi$ -orbital of the central molecule near  $E_F$  as shown in the spin-polarized differential LDOS of Figure 3a. To further examine the  $\pi$ -

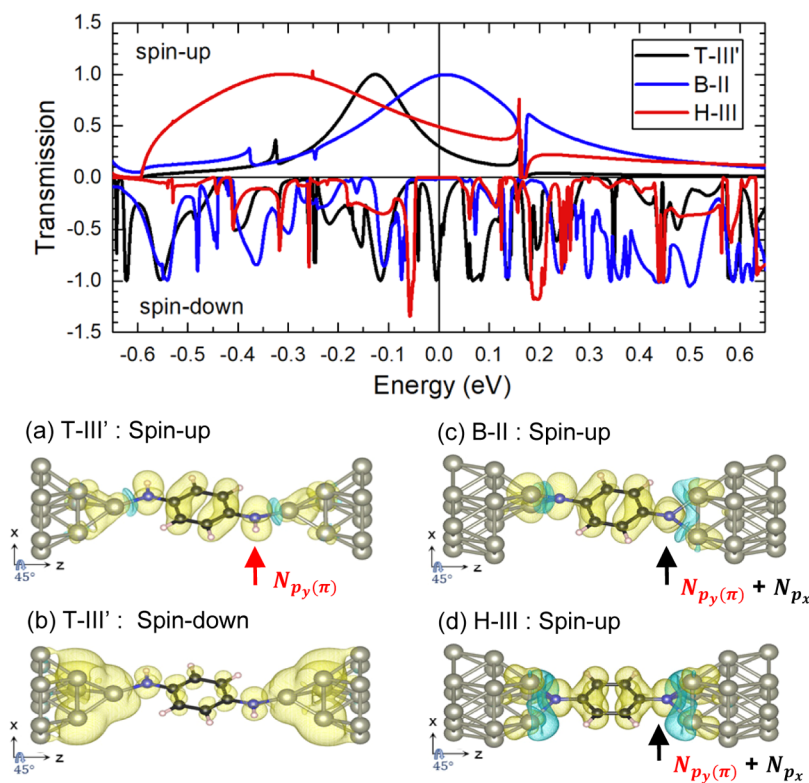


**Figure 2.** Top: spin-polarized transmission spectra for the T-III', B-II, and H-III cases in the parallel magnetic configuration. Bottom: differential LDOS, which is defined as  $\text{LDOS}(\text{Co/BDA/Co junction}) - \text{LDOS}(\text{Co/vacuum/Co junction})$  for (a) spin-up and (b) spin-down channels of the T-III' case, (c) spin-up channel of the B-II case, and (d) spin-up channel of the H-III case in an energy interval of  $-0.3$  to  $0.2$  eV. Yellow (blue) represents the positive (negative) magnitude of differential LDOS. Here, we simply remove the central molecule to form Co/vacuum/Co junction.

resonant spin-up channel, we artificially disrupt the H-atom of the B-II+H case to form a fake dissociated B-II+H-ADH case without doing any structural relaxation. Interestingly, the top panel of Figure 3 reveals that the pronounced  $\pi$ -resonant spin-up transmission feature disappears in the B-II+H case but appears again in the B-II+H-ADH case when an additional H-atom is artificially removed and the N-atom tends to combine with the Co-d orbital, as displayed in Figure 3b.

Moreover, we insert methylene ( $\text{CH}_2$ ) units between the N-atom and the phenyl ring to form the 1,4-benzenedimethanamine molecule (BDMA case). The structural relaxation causes structural reorientation between Co apex atoms and the central BDMA molecule, as shown in the spin-polarized differential LDOS of Figure 3c. It is intriguing to find that not only the  $\pi$ -resonant spin-up transmission feature but also the spiky spin-down transmission peaks can be dramatically suppressed. Although the strong spin-up hybridization between  $\text{N-p}_{x,y}$  and Co-d orbitals exists around  $-0.65$  eV, as presented in Figure 3d, the N-atom and central phenyl ring are well separated by  $\text{CH}_2$  and hence in turn drastically eliminate spin-polarized resonance channels.

We next turn to the dative contact in H-non-dissociated T-III'+H cases and the fake dissociated T-III'+H-ADH case simply by artificially disrupting the H-atom of the T-III'+H case. Similarly, one can expect that the pronounced  $\pi$ -resonant spin-up transmission feature of the T-III' case is first eliminated by adding a H-ion and can be generated again by artificially removing the H-ion, as presented in Figure 4a. Meanwhile, the much larger N-Co bond length in the nondissociated T-III'+H case, that is,  $d_{\text{N-Co}}$  is  $1.84$  Å (T-III') and  $2.05$  Å (T-III'+H), not only eliminates spin-up trans-

mission feature near below  $E_{\text{F}}$ , that is,  $\Delta_{\text{+H}}$  in Figure 4g, but also presents the unoccupied 4-fold molecular orbital of the central molecule, that is,  $\Delta 1$ ,  $\Delta 2$ ,  $\nabla 1$ , and  $\nabla 2$  in Figure 4c–f, which are about 5 times larger than ordinary occupied 2-fold  $\Delta_{\text{+H}}$ , which contributed to  $\pi$ -resonant spin-up transmission in previous discussed H-dissociated cases.

To further distinguish how the H-dissociation onto the N-linker affects the spinterface effect in Co/BDA/Co SMMJs, we present in Figure 5a–e the DOSs and LDOSs for (a) isolated BDA molecule, (b) isolated BDA (2H) molecule directly extracted from the nondissociated TIII'+H case and (c) nondissociated T-III'+H case itself, and (d) isolated BDA (1H) molecule directly extracted from the dissociated T-III' case and (e) dissociated T-III' junction case itself. Comparing to the 2-fold HOMO and HOMO  $- 1$  levels and 4-fold LUMO and LUMO  $+ 1$  levels of the perfect BDA molecule, the reconstruction of  $\text{NH}_2$  of the BDA (2H) molecule renders the split of HOMO and HOMO  $- 1$  (LUMO and LUMO  $+ 1$ ) levels. Moreover, the Co-BDA (2H) molecule in contact with Co NWs moves all four molecular levels toward lower energies. Since the LUMO and LUMO  $+ 1$  levels are shifted closer to  $E_{\text{F}}$ , corresponding to the  $\Delta 1$  and  $\Delta 2$  energy levels, respectively, as shown in Figure 4a, their 4-fold molecular orbital, which is mainly contributed by the phenyl ring, can efficiently block the spin injection from the Co electrode. Instead, once we remove one H-ion to form Co-BDA (1H) molecules, the broad spin-up 2-fold HOMO level is located at  $E_{\text{F}}$  and dominates the  $\pi$ -resonant spin-up transmission of the T-III' case, as shown in Figure 2. Therefore, our results reveal that nondissociation (dissociation) of the H-ion onto the N-linker dramatically blocks (allows) the spin injection from the

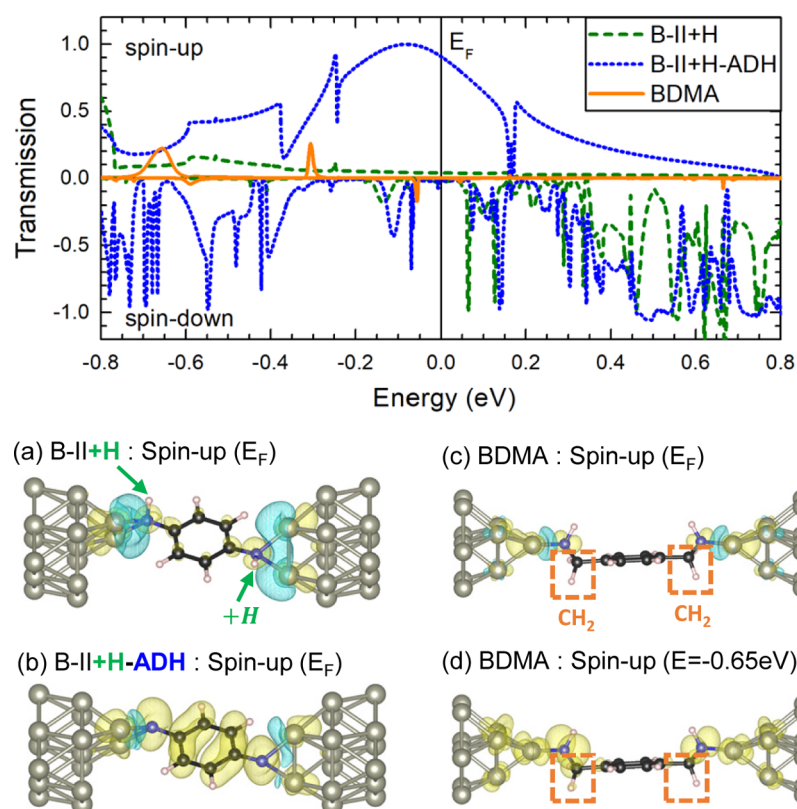


**Figure 3.** Top: spin-polarized transmission spectra for the B-II+H and BDMA cases in the parallel magnetic configuration. Bottom: differential LDOS, which is defined as  $\text{LDOS}(\text{Co/BDA/Co junction}) - \text{LDOS}(\text{Co/vacuum/Co junction})$ , for the spin-up channel at  $E_F$  of (a) B-II+H case, (b) B-II+H-ADH case, and (c) BDMA case and for (d) spin-up channel of the BDMA case at  $-0.65$  eV. Yellow (blue) represents the positive (negative) magnitude of differential LDOS. Here, we simply remove the central molecule to form Co/vacuum/Co junction.

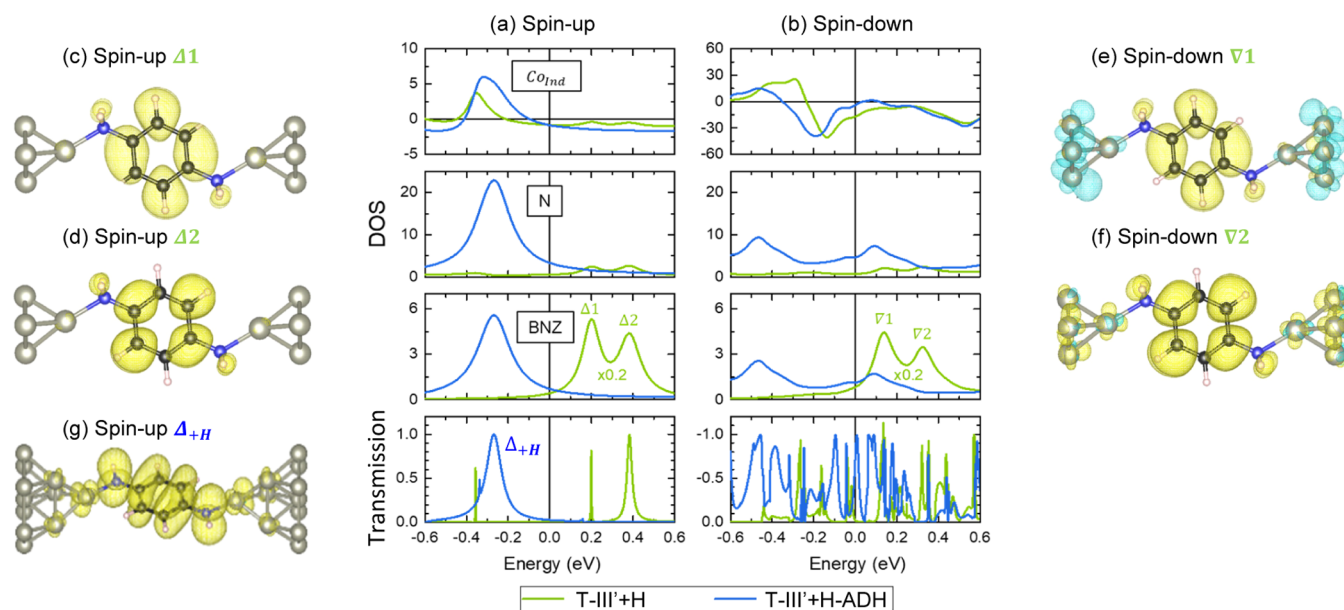


**Figure 4.** (a) Spin-up and (b) spin-down DOS and transmission for the T-III'+H and T-III'+H-ADH cases in the parallel magnetic configuration, where the DOS ( $\text{Co}_{\text{ind}}$ ) is defined as  $\text{DOS}(\text{Co/BDA/Co junction}) - \text{DOS}(\text{Co/vacuum/Co junction})$ . The differential LDOSs for (c)  $\Delta_1$  and (d)  $\Delta_2$  spin-up features and for (e)  $\nabla_1$  and (f)  $\nabla_2$  spin-down features in the T-III'+H case. The differential LDOS for (g)  $\Delta_{+H}$  spin-up feature in the T-III'+H-ADH case.

Co electrode into the central molecule and thus in turn destroys (assists) the spinterface effect via the hybridization between Co-d, N- $p$ , and the  $\pi$ -orbital of the central phenyl ring.

## CONCLUSIONS

In conclusion, the first-principles calculation with the NEGF method is applied to demonstrate that the contact geometry and the interfacial bond mechanism, which are crucial to

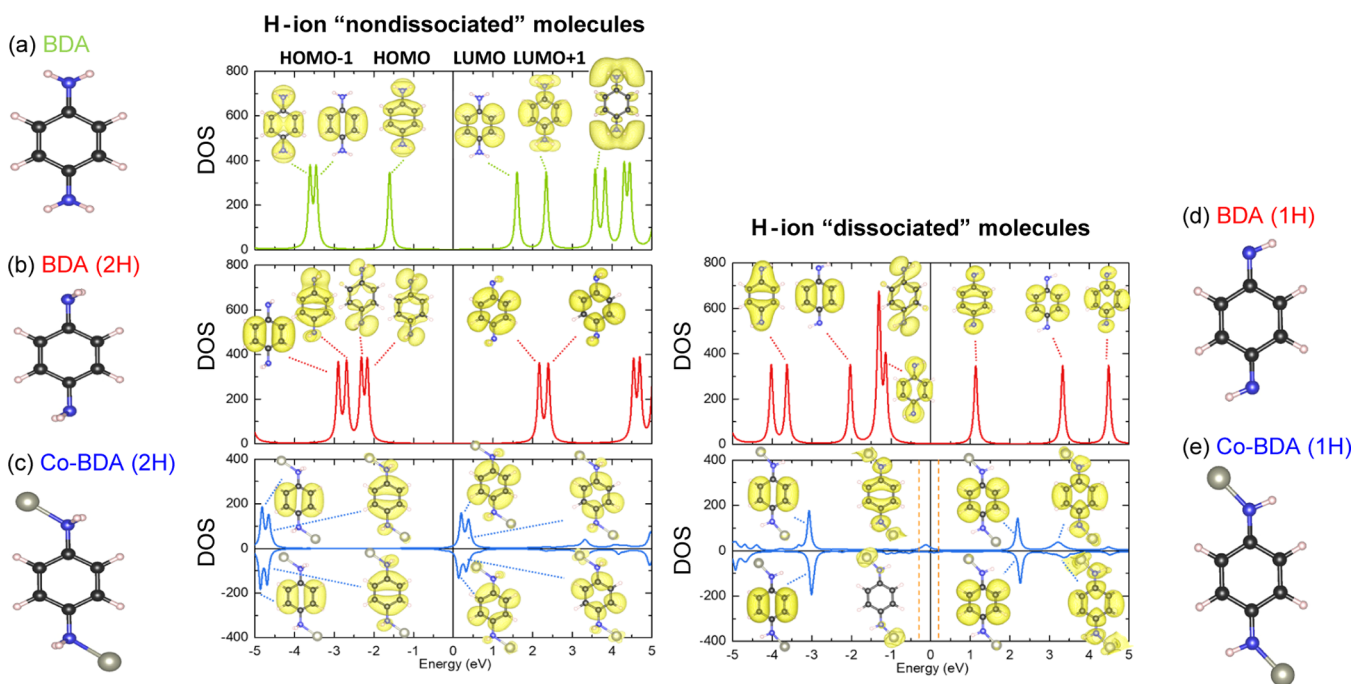


**Figure 5.** DOSs and LDOSs for (a) isolated BDA molecule, (b) isolated BDA (2H) molecule artificially extracted from the nondissociated T-III'+H case and (c) nondissociated T-III'+H case itself, and (d) isolated BDA (1H) molecule artificially extracted from the dissociated T-III' case and (e) dissociated T-III' junction case itself.

control the interface transparency to spin transport in amine-ended SMMJs. The covalent bonding between the H-dissociated amine linker and spin-polarized Co apex atoms can preserve the spin-up pronounced resonance channel regardless of the choice of contact sites, that is, the T-III', B-II, and H-III cases. However, the dative contact is proposed in the H-non-dissociated B-II+H and T-III'+H cases, and their enlarged interfacial Co–N bond lengths not only destroy the spinterface effect but also block the spin injection. The underlying mechanism can be understood by the fact that the strong (weak) hybridization between Co-d, N- $p_y$ , and the  $\pi$ -orbital of the central phenyl ring in H-dissociated (H-non-dissociated) amine-ended SMMJs renders the 2-fold HOMO (4-fold LUMO) of the central molecule closer to the Fermi energy. This theoretical work may provide more insights to illustrate the spin transport property in real SMMJs, since the contact geometries and interfacial bond mechanisms remain unclear during the breaking junction technique.

## AUTHOR INFORMATION

### Corresponding Author

Yu-Hui Tang – Department of Physics, National Central University, Jung-Li 32001, Taiwan; [orcid.org/0000-0002-3579-6753](https://orcid.org/0000-0002-3579-6753); Email: [yhtang@cc.ncu.edu.tw](mailto:yhtang@cc.ncu.edu.tw)

### Author

Kuan-Rong Chiang – Department of Physics, National Central University, Jung-Li 32001, Taiwan

Complete contact information is available at:

<https://pubs.acs.org/10.1021/acsomega.1c00930>

### Notes

The authors declare no competing financial interest.

## ACKNOWLEDGMENTS

We thank Prof. Chun-Guey Wu for her helpful advice. We thank the National Center for High-performance Computing (NCHC) of National Applied Research Laboratories (NAR-Labs) in Taiwan for providing computational and storage resources. This work was supported by the Ministry of Science and Technology (MOST 106-2112-M-008-011 and 108-2628-M-008-004-MY3) and the National Center for Theoretical Sciences (NCTS).

## REFERENCES

- (1) Tsutsui, M.; Taniguchi, M. Single Molecule Electronics and Devices. *Sensors* **2012**, *12*, 7259–7298.
- (2) Ratner, M. A brief history of molecular electronics. *Nat. Nanotechnol.* **2013**, *8*, 378–381.
- (3) Aradhya, S. V.; Venkataraman, L. Single-molecule junctions beyond electronic transport. *Nat. Nanotechnol.* **2013**, *8*, 399–410.
- (4) Kiguchi, M.; Kaneko, S. Single molecule bridging between metal electrodes. *Phys. Chem. Chem. Phys.* **2013**, *15*, 2253–2267.
- (5) Huang, C.; Rudnev, A. V.; Hong, W.; Wandlowski, T. Break junction under electrochemical gating: testbed for single-molecule electronics. *Chem. Soc. Rev.* **2015**, *44*, 889–901.
- (6) Wan, H.; Zhou, B.; Chen, X.; Sun, C. Q.; Zhou, G. Switching, Dual Spin-Filtering Effects, and Negative Differential Resistance in a Carbon-Based Molecular Device. *J. Phys. Chem. C* **2012**, *116*, 2570–2574.
- (7) Wan, H.; Xu, Y.; Zhou, G. Dual conductance, negative differential resistance, and rectifying behavior in a molecular device modulated by side groups. *J. Chem. Phys.* **2012**, *136*, 184704.
- (8) Su, T. A.; Neupane, M.; Steigerwald, M. L.; Venkataraman, L.; Nuckolls, C. Chemical principles of single-molecule electronics. *Nat. Rev. Mater.* **2016**, *1*, 16002.
- (9) Xu, B. Q.; Li, X. L.; Xiao, X. Y.; Sakaguchi, H.; Tao, N. J. Electromechanical and Conductance Switching Properties of Single Oligothiophene Molecules. *Nano Lett.* **2005**, *5*, 1491–1495.
- (10) Tao, N. J. Electron transport in molecular junctions. *Nat. Nanotechnol.* **2006**, *1*, 173–181.

- (11) Martin, C. A.; Ding, D.; van der Zant, H. S. J.; van Ruitenbeek, J. M. Lithographic mechanical break junctions for single-molecule measurements in vacuum: possibilities and limitations. *New J. Phys.* **2008**, *10*, 065008.
- (12) Dubois, L. H.; Nuzzo, R. G. Synthesis Structure, and Properties of Model Organic Surfaces. *Annu. Rev. Phys. Chem.* **1992**, *43*, 437–463.
- (13) Ulman, A. Formation and Structure of Self-Assembled Monolayers. *Chem. Rev.* **1996**, *96*, 1533–1554.
- (14) Pearson, R. G. Hard and Soft Acids and Bases. *J. Am. Chem. Soc.* **1963**, *85*, 3533–3539.
- (15) Li, Z.; Kosov, D. S. Nature of well-defined conductance of amine-anchored molecular junctions: Density functional calculations. *Phys. Rev. B: Condens. Matter Mater. Phys.* **2007**, *76*, 035415.
- (16) Kamenetska, M.; Koentopp, M.; Whalley, A. C.; Park, Y. S.; Steigerwald, M. L.; Nuckolls, C.; Hybertsen, M. S.; Venkataraman, L. Formation and Evolution of Single-Molecule Junctions. *Phys. Rev. Lett.* **2009**, *102*, 126803.
- (17) Sugita, Y.; Taninaka, A.; Yoshida, S.; Takeuchi, O.; Shigekawa, H. The effect of nitrogen lone-pair interaction on the conduction in a single-molecule junction with amine-Au bonding. *Sci. Rep.* **2018**, *8*, 5222.
- (18) Kim, Y.; Hellmuth, T. J.; Bürkle, M.; Pauly, F.; Scheer, E. Characteristics of Amine-Ended and Thiol-Ended Alkane Single-Molecule Junctions Revealed by Inelastic Electron Tunneling Spectroscopy. *ACS Nano* **2011**, *5*, 4104–4111.
- (19) Sheng, W.; Li, Z. Y.; Ning, Z. Y.; Zhang, Z. H.; Yang, Z. Q.; Guo, H. Quantum transport in alkane molecular wires: Effects of binding modes and anchoring groups. *J. Chem. Phys.* **2009**, *131*, 244712.
- (20) Ning, Z.-Y.; Qiao, J.-S.; Ji, W.; Guo, H. Correlation of interfacial bonding mechanism and equilibrium conductance of molecular junctions. *Front. Phys.* **2014**, *9*, 780–788.
- (21) Quek, S. Y.; Venkataraman, L.; Choi, H. J.; Louie, S. G.; Hybertsen, M. S.; Neaton, J. B. Amine Gold Linked Single-Molecule Circuits: Experiment and Theory. *Nano Lett.* **2007**, *7*, 3477–3482.
- (22) Sanvito, S. MOLECULAR SPINTRONICS The rise of spinterface science. *Nat. Phys.* **2010**, *6*, 562–564.
- (23) Ruden, P. ORGANIC SPINTRONICS Interfaces are critical. *Nat. Mater.* **2011**, *10*, 8–9.
- (24) Li, D.; Dappe, Y. J.; Smogunov, A. Perfect spin filtering by symmetry in molecular junctions. *Phys. Rev. B* **2016**, *93*, 201403.
- (25) Ning, Z.; Zhu, Y.; Wang, J.; Guo, H. Quantitative Analysis of Nonequilibrium Spin Injection into Molecular Tunnel Junctions. *Phys. Rev. Lett.* **2008**, *100*, 056803.
- (26) Smogunov, A.; Dappe, Y. J. Symmetry-Derived Half-Metallicity in Atomic and Molecular Junctions. *Nano Lett.* **2015**, *15*, 3552–3556.
- (27) Xiong, Y.-C.; Zhou, W.-H.; Nan, N.; Ma, Y.-N.; Li, W. Synchronously voltage-manipulable spin reversing and selecting assisted by exchange coupling in a monomeric dimer with magnetic interface. *Phys. Chem. Chem. Phys.* **2020**, *22*, 422–429.
- (28) Li, D.; Smogunov, A. Giant magnetoresistance due to orbital-symmetry mismatch in transition metal benzene sandwich molecules. *Phys. Rev. B* **2021**, *103*, 085432.
- (29) Tang, Y.-H.; Lin, C.-J. Strain-Enhanced Spin Injection in Amine-Ended Single-Molecule Magnetic Junctions. *J. Phys. Chem. C* **2016**, *120*, 692–696.
- (30) Li, D. Highly conductive and complete spin filtering of nickel atomic contacts in a nitrogen atmosphere. *Phys. Rev. B* **2019**, *99*, 174438.
- (31) Tang, Y. H.; Lin, C. J.; Chiang, K. R. Hard-hard coupling assisted anomalous magnetoresistance effect in amine-ended single-molecule magnetic junction. *J. Chem. Phys.* **2017**, *146*, 224701.
- (32) Tang, Y.-H.; Huang, B.-H. Manipulation of Giant Field-Like Spin Torque in Amine-Ended Single-Molecule Magnetic Junctions. *J. Phys. Chem. C* **2018**, *122*, 20500–20505.
- (33) Kresse, G.; Hafner, J. Ab initio molecular dynamics for liquid metals. *Phys. Rev. B: Condens. Matter Mater. Phys.* **1993**, *47*, 558–561.
- (34) Kresse, G.; Hafner, J. Ab initio molecular dynamics for open-shell transition metals. *Phys. Rev. B: Condens. Matter Mater. Phys.* **1993**, *48*, 13115–13118.
- (35) Kresse, G.; Hafner, J. Ab initio molecular-dynamics simulation of the liquid-metal–amorphous-semiconductor transition in germanium. *Phys. Rev. B: Condens. Matter Mater. Phys.* **1994**, *49*, 14251–14269.
- (36) Kresse, G.; Furthmüller, J. Efficiency of ab-initio total energy calculations for metals and semiconductors using a plane-wave basis set. *Comput. Mater. Sci.* **1996**, *6*, 15–50.
- (37) Perdew, J. P.; Burke, K.; Ernzerhof, M. Generalized Gradient Approximation Made Simple. *Phys. Rev. Lett.* **1996**, *77*, 3865–3868.
- (38) Waldron, D.; Liu, L.; Guo, H. Ab initio simulation of magnetic tunnel junctions. *Nanotechnology* **2007**, *18*, 424026.
- (39) Taylor, J.; Guo, H.; Wang, J. Ab initio modeling of quantum transport properties of molecular electronic devices. *Phys. Rev. B: Condens. Matter Mater. Phys.* **2001**, *63*, 245407.
- (40) Ke, Y.; Xia, K.; Guo, H. Disorder Scattering in Magnetic Tunnel Junctions: Theory of Nonequilibrium Vertex Correction. *Phys. Rev. Lett.* **2008**, *100*, 166805.